J Therm Anal Calorim (2012) 107:335–344
DOI 10.1007/s10973-011-1835-8

Thermal and spectroscopic data to investigate the oxamic acid, sodium oxamate and its compounds with some bivalent transition metal ions

F. J. Caires · L. S. Lima · C. T. Carvalho · A. B. Siqueira · Oswaldo Treu-Filho · M. Ionashiro

Received: 29 October 2010 / Accepted: 28 July 2011 / Published online: 11 August 2011

Abstract Synthesis, characterization, and thermal behavior of transition metal oxamates, $M(NH_2C_2O_3)_2{\cdot}nH_2O$ (M = Mn(II), Fe(II), Co(II), Ni(II), Cu(II), Zn(II)), as well as the thermal behavior of oxamic acid and its sodium salt ($NaNH_2C_2O_3$) were investigated employing simultaneous thermogravimetry and differential scanning calorimetry (TG-DSC), experimental and theoretical infrared spectroscopy, TG-DSC coupled to FTIR, elemental analysis and complexometry. The results led to information about the composition, dehydration, thermal stability, thermal decomposition, as well as of the gaseous products evolved during the thermal decomposition of these compounds in dynamic air and N_2 atmospheres.

Keywords Bivalent transition metal · Oxamate · Thermal behavior · Theoretical calculations

Introduction

Complexes of ligands containing both carboxylic acid and amide have not been widely studied on solid state. The simplest of these ligands is oxamic acid ($NH_2COCOOH$, H_2oxam), and it is well known as being a versatile ligand, which may to act as bidentate, tridentate, or tetradentate (bridging ligand) in respect to the number of coordination and as mono or diamin, in respect to its charge. However, a few articles have been published on oxamate complexes.

Preparation and investigation of several metal-ion oxamates have been investigated in the solid state using thermoanalytical techniques, X-ray diffractometry, infrared spectroscopy, and so on. The articles published are concerned with the infrared and far-infrared spectra of solid oxamic acid, deutero-oxamic acid and their salts [1], complexes of zinc group metals with oxamic acid [2], infrared and electronic spectra of the complexes of oxamic acid with Ni(II) [3], thermal, spectral and magnetic studies of oxamic acid compounds of cobalt(II), nickel(II) and copper(II) ions [4], synthesis, spectroscopic and thermal study of oxamic acid compounds of some metal(III) ions [5], thermal analysis of oxamates, thio-oxamates and their complexes [6, 7], and a new eight-coordinate complex of manganese(II) compound containing oxamate and water molecules [8]. Thermogravimetric, differential thermal analysis, and thermogravimetry, and differential scanning calorimetry (TG-DSC) coupled to FTIR spectroscopies have been used to characterize complexes of bivalent transition metal ions [9, 10]. However, they are not found in the literature thermal studies involving all metal-ions with oxamates, as well as the characterization of the gaseous products released during the thermal decomposition.

For the infrared spectroscopy study, the experimental infrared spectrum was compared with the theoretical infrared one which was realized by ab initio calculations. Extensive experimental and theoretical investigations have been focused on elucidating the structure and normal vibrations of compounds [11]. Thus, calculations of the optimal molecular geometry and vibrational frequency of oxamic acid, sodium

F. J. Caires (✉) · L. S. Lima · O. Treu-Filho · M. Ionashiro
Instituto de Química, UNESP, CP 355, Araraquara, SP 14801-970, Brazil
e-mail: caires.flavio@yahoo.com.br

C. T. Carvalho
Universidade Federal da Grande Dourados, UFGD, Rodovia-Itahum, km 12, Dourados, MS 79804-970, Brazil

A. B. Siqueira
Instituto de Ciências Exatas e da Terra, Campus Pontal do Araguaia, UFMT, MT-100, Rodovia, MT 78698-000, Brazil

oxamate, and manganese oxamate were made. The density functional theory (DFT) calculations are reported to provide excellent vibrational frequencies of organic compounds if the calculated frequencies are scaled to compensate for the approximate treatment of electron correlation for basis set deficiencies and anharmonicity [12].

In this article, the objective of the present research was to investigate the thermal behavior of oxamic acid, its sodium salt, and to prepare solid-state compounds of some bivalent transition metal oxamates (Mn, Fe, Co, Ni, Cu and Zn) and to characterize and to investigate by means of complexometry, elemental analysis, infrared spectroscopy (FTIR), simultaneous TG-DSC, and TG-DSC coupled to FTIR.

Experimental

The oxamic acid, $H_2NCOCOOH$, with 99% purity was obtained from Sigma. Carbonates of Mn(II), Fe(II), Co(II), Ni(II), Cu(II) and Zn(II) were prepared as described in earlier paper [13].

Solid-state compounds of these metal ions were prepared by mixing the corresponding metal carbonate in slight excess maintained in aqueous suspension with oxamic acid. The aqueous suspension was heated slowly up to near ebullition, cooled to room temperature, and filtered to remove the carbonate in excess. Thus, the aqueous solutions of the respective metal oxamates were evaporated to near dryness in water bath, dried in a forced circulation oven at 50 °C during overnight, and removed to a desiccator over anhydrous calcium chloride.

In the solid-state compounds, metal ions, hydration water and oxamate contents were determined from TG curves. The metal ions were also determined by complexometry with standard EDTA solution [14, 15], after igniting the compounds to the respective oxides and their dissolution in hydrochloric acid solution.

Carbon, hydrogen, and nitrogen contents were determined by microanalytical procedures, with EA 1110 CHNS-0 Elemental Analyzer from CE Instruments.

The attenuate total reflectance infrared spectra of sodium oxamate, as well as of its metal-ion compounds were recorded on a Nicolet iS10 FTIR spectrophotometer, using an ATR accessory with a Ge window. IR spectra were also recorded with samples pressed into KBr pellets, within 4,000–600 cm^{-1}.

Simultaneous TG-DSC curves were obtained with a Thermogravimetric Analyzer STARe system from Mettler Toledo. The purge gas was air or nitrogen, with a flow of 50 mL min^{-1}, a heating rate of 20 °C min^{-1} and samples weighing about 7 mg. Alumina crucibles were used for recording the TG-DSC curves.

The TGA-FTIR experiments were performed using a Thermogravimetric Analyzer Mettler TG-DSC, coupled with a Nicolet iS10 FTIR Spectrometer equipped with an IR gas cell. The transfer line consists of a stainless steel tube of 120 cm in length (2 mm in inner diameter) heated at a constant temperature of 250 °C. FTIR measurements were carried out with a DTGS detector in a specifically developed gas cell, heated at a constant temperature of 200 °C. The interferometer and the gas cell compartments were purged with high purified N_2.

Computational strategy

In the present investigation, the employed quantum chemical approach to determining the molecular structures was Becke three-parameter hybrid method using Lee-Yang-Par correlation functional [16, 17], and the basis sets used for calculations were the 6-311 g(d) [18, 19]. The performed molecular calculations in this study were done using the Gaussian 09 routine [20].

Theoretical infrared spectrum was calculated using a harmonic field [21], based on C_1 symmetry (electronic state ^1A). Frequency values (not scaled), relative intensities, assignments and description of vibrational modes are presented. The calculations of vibrational frequencies were also implemented to determine an optimized geometry that constitutes minimum or saddle points. The principal infrared active fundamental modes assignments and descriptions were done using Gauss View 5.0.8 graphics routine [22].

Results and discussion

The TG-DSC curves and IR spectrum of the gases released during the thermal decomposition of oxamic acid in dynamic air and nitrogen atmospheres are shown in the Figs. 1a, b and 2a, b, respectively. The TG curve in both the atmospheres shows that the oxamic acid is thermally stable up to 140 °C, and above this temperature the thermal decomposition begins through a fast process up to 250 °C (air) and 270 °C (N_2) with mass loss of 95%, followed by a slow process up to 520 °C (air) and 600 °C (N_2), with total mass loss. Corresponding to the mass loss in both atmospheres, the DSC curve shows an endothermic peak attributed to fusion/evaporation and decomposition of oxamic acid.

Test with sample heated up to 250 °C in an alumina crucible sheltered by a glass tube in a digital melting point equipment, and a heating rate of 20 °C min^{-1}, firstly sublimation, followed by fusion and condensation of the evaporated product in the glass tube wall were observed. The condensated product was identified as oxamic acid and

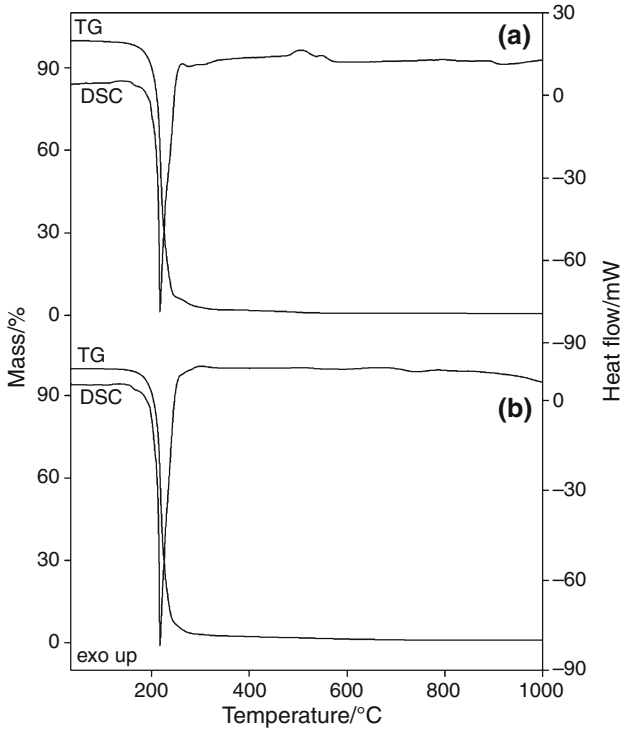

Fig. 1 Simultaneous TG-DSC curves of the oxamic acid in **a** air (m = 7.185) and **b** N_2 (m = 7.089 mg), atmospheres

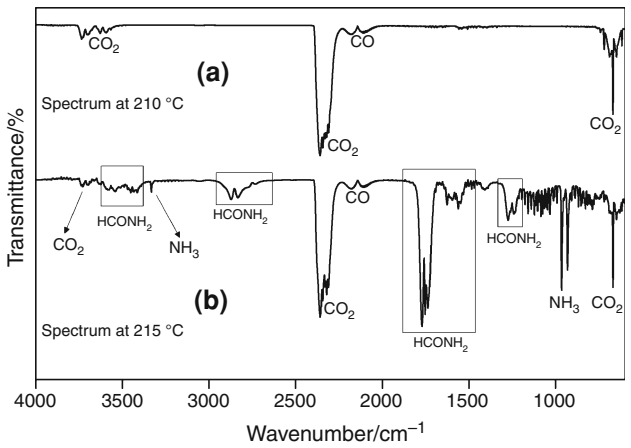

Fig. 2 IR spectra of the gases released during the decomposition of oxamic acid in **a** air and **b** N_2, atmospheres

formamide using infrared spectroscopy. The gaseous products evolved during the thermal decomposition of oxamic acid, in dry air and N_2 atmospheres, were also monitored by FTIR, and it has carbon monoxide and dioxide as main products (air) or carbon monoxide and dioxide, ammonia and formamide (N_2). Thus, the mass loss corresponding to the endothermic peak is because of sublimation, fusion and thermal decomposition of the oxamic acid, with releasing of CO, CO_2 (air) and CO, CO_2, NH_3 and formamide (N_2) in disagreement with the Ref. [4].

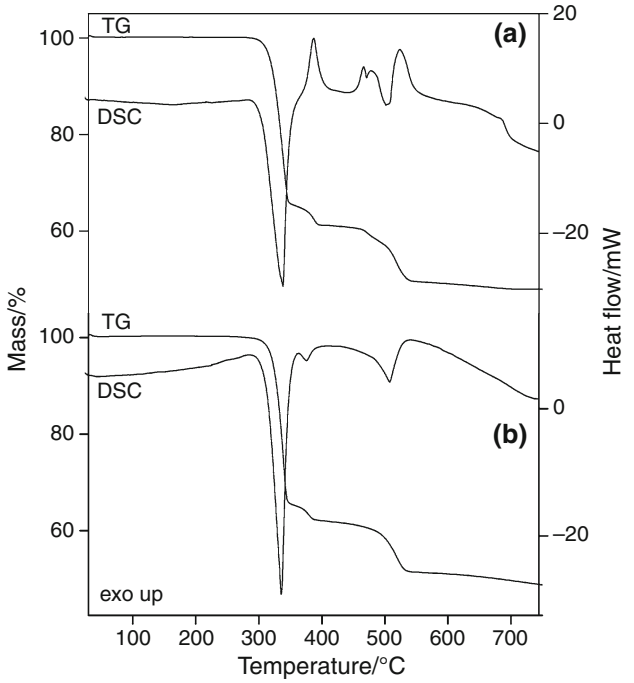

Fig. 3 Simultaneous TG-DSC curves of the sodium oxamate in **a** air (m = 7.092) and **b** N_2 (m = 7.051 mg), atmospheres

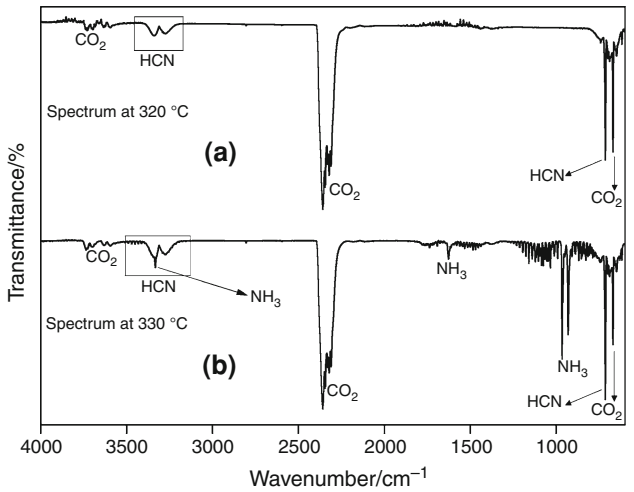

Fig. 4 IR spectra of the gases released during the decomposition of sodium oxamate in **a** air and **b** N_2, atmospheres

For the anhydrous sodium oxamate, the TG-DSC curves and IR of the gases released during the thermal decomposition in dynamic dry air and nitrogen atmospheres are shown in Figs. 3a, b and 4a, b, respectively. These curves show that the anhydrous compound is stable up to 290 °C, and above this temperature the thermal decomposition occurs in four steps in both atmospheres.

In dynamic dry air atmosphere, the steps of thermal decomposition occur between 290–345, 345–390, 440–530,

and 530–700 °C, corresponding to an endothermic peak at 340 °C (decomposition) and exothermic peaks at 385, 465, 480, and 520 °C (oxidation of evolved gaseous products), with losses of 34.19, 4.82, 10.88, and 2.03%, respectively, with the formation of sodium carbonate, as residue.

In dynamic dry nitrogen atmosphere, the steps of thermal decomposition occur between 290–340, 340–380, 380–530, and 530 ≥ 740 °C, corresponding to endothermic peaks at 330, 370, and 530 °C, with losses of 34.59, 3.54, 9.83, and 3.34%, respectively, with formation of sodium carbonate and a carbonaceous residue.

In both the atmospheres, no thermal event corresponding to the last mass loss is observed in the DSC curve, probably because the thermal decomposition occurs slowly and the heat involved in this step is not sufficient to produce a thermal event.

The TG curve also shows a level after the first two mass losses (390–440 °C), indicating the formation of a stable intermediate. Tests with sample heated up to 400 °C, and permitted to verify the formation of oxalate as intermediate and presence of carbonaceous residue.

The gaseous products which were evolved during the thermal decomposition of the sodium oxamate in dynamic dry air and nitrogen atmospheres were monitored by FTIR, and it has cyanhydric acid, ammonia, and carbon dioxide in the first step and ammonia, carbon monoxide, and dioxide in the last three steps.

For the synthesized compounds, the analytical and thermoanalytical (TG) data are shown in Table 1. These results establish the stoichiometry of these compounds, which are in agreement with the general formula $M(NH_2C_2O_3)_2{\cdot}nH_2O$, where *M* represents Mn(II), Fe(II), Co(II), Ni(II), Cu(II) and Zn(II), $NH_2C_2O_3$ is oxamate, and $n = 0$ (Mn), 1 (Cu, Zn), 1.5 (Co, Ni) or 2 (Fe).

The oxamic dimer acid, sodium oxamate and manganese oxamate structures were optimized and theoretical frequency, assignments and description were calculated. The optimized structures result in theoretically computed energies (a. u.) equals at −717.17006136 (oxamic acid), −520.35342267 (sodium oxamate) and −1866.98992164 (manganese oxamate) and the optimized structures are shown in Fig. 5. These results are in agreement between the experimental and theoretical IR spectra calculated in B3LYP/6-311^{++}G* level.

The representative experimental and calculated spectra of the compounds are shown in Fig. 6 and Table 2. Assessing the energies and the theoretical IR spectra of different structures can be observed an interaction of the amide group in the formation of dimers and coordination of the metal with the ligand. The theoretical vibrational bands observed in the infrared region are very sharp, broad, and less intense. All these bands have been assigned in terms of various fundamental, overtone and combination vibrations. The calculated frequencies are slightly higher than that of the observed values for the majority of the normal modes. The major factor responsible for these discrepancies between the experimental and computed value is related to the fact that the experimental value is anharmonic frequency, while the calculated value is harmonic frequency. While anharmonic is the main factor of the discrepancies in the case of vibrations related to the C–H, N–H, or O–H bonds, for other vibrations most of the discrepancies come from the approximate nature of the used computational technique, and probably also from the lattice effects in the substance studied as a solid [23].

The two strong bands at 3,358 and 3,242 cm^{-1} are assigned as asymmetric and symmetric stretching vibrations of the NH_2 group. The assignment of the $\nu_{s(NH_2)}$ is more complicated because of overtones and combination bands of the amide and carboxylate functional groups, it appears as a rather broad band with a maximum at 3,242 cm^{-1} in the IR.

The C=O absorption of amides occurs at lower frequencies than that of the normal carbonyl absorption because of the resonance effect. For example, the $\nu_{(C=O)}$ of oxamic acid is 1,676 cm^{-1}. The antisymmetric stretching modes of the carboxylate and amide groups are

Table 1 Analytical and thermoanalytical TG* data for the $M(NH_2C_2O_3)_2{\cdot}nH_2O$ compounds

Compound	Metal oxide/%			L (lost)/%		H_2O/%		C/%		N/%		H/%		Final residue
	Calcd.	EDTA	TG	Calcd.	TG	Calcd.	TG	Calcd.	E. A.	Calcd.	E. A.	Calcd.	E. A.	TG
$Mn(L)_2$	33.01	32.38	32.86	66.99	67.14	–	–	20.79	20.85	12.13	11.93	1.75	1.82	Mn_3O_4
$Fe(L)_2{\cdot}H_2O$	29.80	29.37	30.20	56.75	56.60	13.45	13.20	17.93	18.01	10.46	10.50	3.02	2.98	Fe_2O_3
$Co(L)_2{\cdot}1.5H_2O$	30.63	30.37	30.81	59.06	58.79	10.31	10.40	18.33	18.00	10.69	10.50	2.70	3.01	Co_3O_4
$Ni(L)_2{\cdot}1.5H_2O$	28.53	28.75	28.40	61.15	61.40	10.32	10.20	18.35	18.10	10.70	11.02	2.70	3.05	NiO
$Cu(L)2{\cdot}1H_2O$	30.87	30.94	31.00	62.14	62.16	6.99	6.84	18.64	18.80	6.99	7.15	2.35	2.30	CuO
$Zn(L)_2{\cdot}1H_2O$	31.36	31.04	31.17	61.70	62.01	6.94	6.82	18.51	18.40	10.80	11.14	2.34	2.04	ZnO

L oxamate, * dynamic air atmosphere

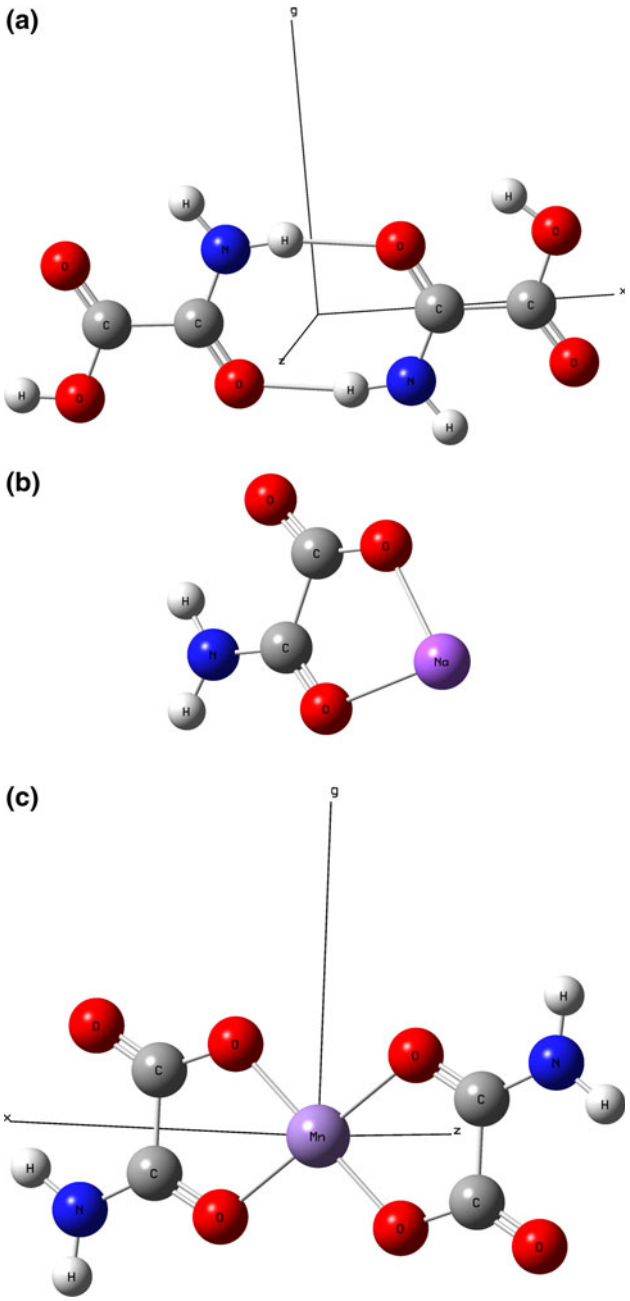

Fig. 5 Theoretical 3D structure of solid-state of the **a** oxamic dimer acid, **b** sodium oxamate and **c** manganese optimized using Becke three-parameter hybrid method, 6-311^{++}G* basis set of Gaussian 09

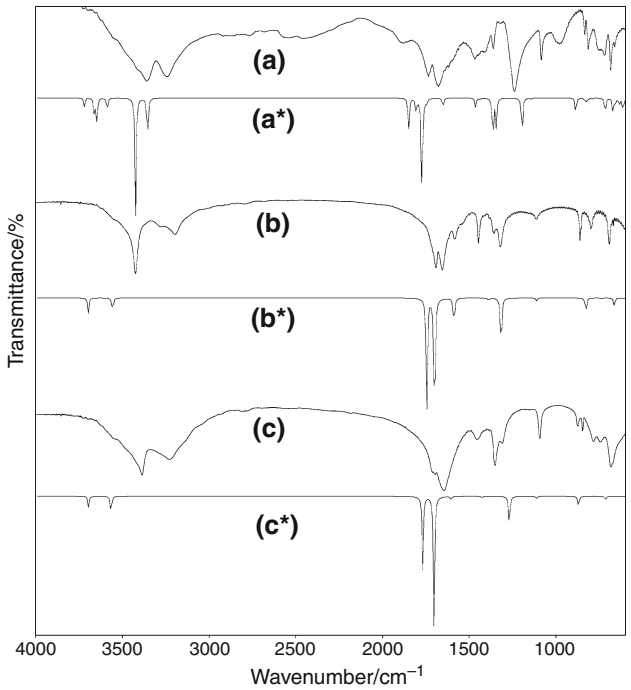

Fig. 6 Experimental (**a**, **b**, **c**) and calculated (**a***, **b***, **c***) IR spectra of **a** oxamic acid, **b** sodium oxamate and **c** manganese oxamate

observed at 1,696; 1,646 cm^{-1} (Mn); 1,700; 1,667 cm^{-1} (Fe); 1,671 cm^{-1} (Co); 1,668; 1,562 cm^{-1} (Ni); 1,713; 1,685 cm^{-1} (Cu); and 1,662 cm^{-1} (Zn). The symmetrical frequencies of the amide and carboxylate groups are observed between 1,342–1,459 and 1,286–1,351 cm^{-1}, respectively. These data show that bands due to the antisymmetric stretching modes of the carboxylate and amide groups are moved to lower frequencies in comparison with the oxamic acid and its sodium salt, suggesting that the metal ions are coordinate by oxygen of amide group and by oxygen of carboxylate group, in agreement with the Refs. [5] and [10].

Simultaneous TG-DSC curves of the compounds in dynamic air and nitrogen atmospheres are shown in Fig. 7a–f, a*–f*, respectively. These curves show mass losses in two, three, four, or five steps, corresponding to endothermic peaks due to dehydration or thermal decomposition and exothermic peaks attributed to oxidation of organic matter, metal or metal ions.

The thermal stability of the hydrate (I) or anhydrous compounds (II) in both the atmospheres, as shown by TG-DSC curves depend on the nature of the metal ion, and they follow the order

I: Fe > Co > Zn > Ni = Cu;
II: Ni > Zn > Mn > Fe > Co > Cu.

The TG-DSC curves also show that the formation of stable anhydrous compounds is observed for manganese, iron, and zinc compounds, while for cobalt, nickel, and copper ones the thermal decomposition occurs immediately after the dehydration.

The thermal behavior of the compounds is also heavily depending on the nature of the metal ion, and therefore the features of each these compounds are discussed individually.

Table 2 Wavenumbers (cm^{-1}), intensities, and assignments of bands occurring in the IR spectra of oxamic acid, sodium oxamate, and manganese oxamate

Vibrational assignments	Oxamic acid		Sodium oxamate		Manganese oxamate	
	Theor.	Exper.	Theor.	Exper.	Theor.	Exper.
$\nu_{(OH)}$	$3{,}719_{vw}$					
$\nu_{as(NH_2)}$	$3{,}661_{vw}$		$3{,}697_{vw}$	$3{,}424_{s}$	$3{,}695_{vw}$	$3{,}386_{s,br}$
$\nu_{(OH)}$	$3{,}587_{vw}$					
$\nu_{s(NH_2)}$	$3{,}423_{s}/3{,}355^{a}_{m}$	$3{,}358/3{,}241_{s,br}$	$3{,}557_{vw}$	$3{,}424_{s}/3280_{m}$	$3{,}565_{vw}$	$3{,}228_{s,br}$
$\nu_{as(COO)} + \delta_{NH_2(scissoring)}$			$1{,}745_{s}$	$1{,}692_{s}$	$1{,}778_{s}/1{,}768_{m}$	1696_{s}
$\nu_{(C=O),acid}$	$1{,}849_{w}/1{,}805_{vw}$	$1{,}697_{over}/1{,}735_{m,br}$				
$\nu_{as(CONH_2)} + \delta_{NH_2(scissoring)}$			$1{,}700_{s}$	$1{,}655_{s}$	$1{,}708_{vw}/1{,}702_{s}$	$1{,}646_{s}$
$\nu_{(C=O),amide}$	$1{,}773_{s}/1{,}747_{vw}$	$1{,}676_{s}$				
$\delta_{NH_2(scissoring)}$	$1{,}651/1{,}631_{vw}$	$1{,}540_{over}$	$1{,}588_{w}$	$1{,}584_{m}$	$1{,}605/1{,}600_{vw}$	$1{,}605_{over}$
$\delta_{(OH)} + \rho_{NH_2}$	$1{,}463/1{,}437_{vw}$	$1{,}361_{w}$				
$\nu_{s(CONH_2)} + \delta_{NH_2(scissoring)}$					$1{,}425/1{,}428_{vw}$	$1{,}457_{vw}$
$\delta_{(OH)} + \rho_{NH_2}$	$1{,}363/1{,}343/1{,}195_{m}$	$1{,}084_{m}$				
$\nu_{s(COO)}$			$1{,}316_{s}$	$1{,}321_{m}$	$1{,}269_{m}/1{,}267_{vw}$	$1{,}351_{m}/1{,}309_{w}$
ρ_{NH_2}			$1{,}112_{vw}$	$1{,}110_{vw}$	111_{vw}	$1{,}092_{m}$
$\tau_{(NH_2)}$	$834/825/821/885_{w}$	814_{w}				
$\nu_{s(cc)}$	$813/791_{vw}$	724_{m}	826_{w}	862_{m}	$864_{vw}/869_{w}$	$874_{w}/845_{w}$
$\omega_{(OH)}$	$715/669_{m}$	$753/718_{m}$				
$\tau_{(NH_2)}$			734_{vw}	$689/688_{vw}$		
ρ_{NH_2}			663_{w}	692_{m}		
$\omega_{(NH_2)}$	612_{m}	$685/661_{m}$				

The theoretical wavenumber were calculated in B3LYP/6-311^{++}G* level

vw very weak, *w* weak, *m* medium, *br* broad, *s* strong, *v* stretching, *vs* sym. stretching, *vas* asym. stretching, δ angular deformation, ρ rocking, τ twisting, ω wagging astretching N–H of dimer

Manganese compound

The simultaneous TG-DSC curves in dynamic air and N_2 atmospheres are shown in Fig. 7a, a*, respectively. In both the atmospheres the anhydrous compound is stable up to 180 °C and above this temperature the thermal decomposition in air atmosphere occurs in two steps between 180–250 and 250–330 °C, with losses of 6.15 and 60.99%, corresponding to the small endothermic peak at 240 °C and a large exothermic one, attributed to the thermal decomposition and oxidation of the organic matter, respectively. The total mass loss up to 330 °C is in agreement with the formation of Mn_3O_4. (Calcd. = 66.97%, TG = 67.14%). The last mass loss between 900 and 940 °C, corresponding to an endothermic peak at 930 °C is assigned to the reduction reaction of Mn_3O_4 to MnO (Calcd. = 2.31%, TG = 1.03%), as already observed during the thermal decomposition of manganese malonate [13].

In N_2 atmosphere, the thermal decomposition occurs in three steps, being the last two overlapping ones between 180–250, 250–355, and 355–440 °C, with losses of 3.64, 34.86 and 29.92%, corresponding to the endothermic peaks at 230, 345 and 380 °C, respectively. The total mass loss up to 440 °C is in agreement with the formation of MnO, as final residue (Calcd. = 69.28%, TG = 68.43%).

Iron compound

The simultaneous TG-DSC curves in dynamic air and N_2 atmospheres are shown in Fig. 7b, b*, respectively. In both the atmospheres, the first mass loss between 135 and 165 °C corresponding to an endothermic peak at 150 °C is due to dehydration with loss of $2H_2O$ (Calcd. = 13.45%, TG = 13.20% (air), 13.13% (N_2)).

For the air atmosphere, the thermal decomposition of the anhydrous compound occurs in two steps between 180–300 (fast process) and 300–600 °C (slow one) with losses of 55.03 and 1.57%, corresponding to a large exothermic peak at 250 °C, attributed to the oxidation reaction of Fe(II) to Fe(III) and organic matter with the formation of small amount of carbonaceous residue. No peak corresponding to the thermal decomposition of the carbonaceous residue is observed in the DSC curve, probably because this step occurs slowly, and consequently the heat involved is not

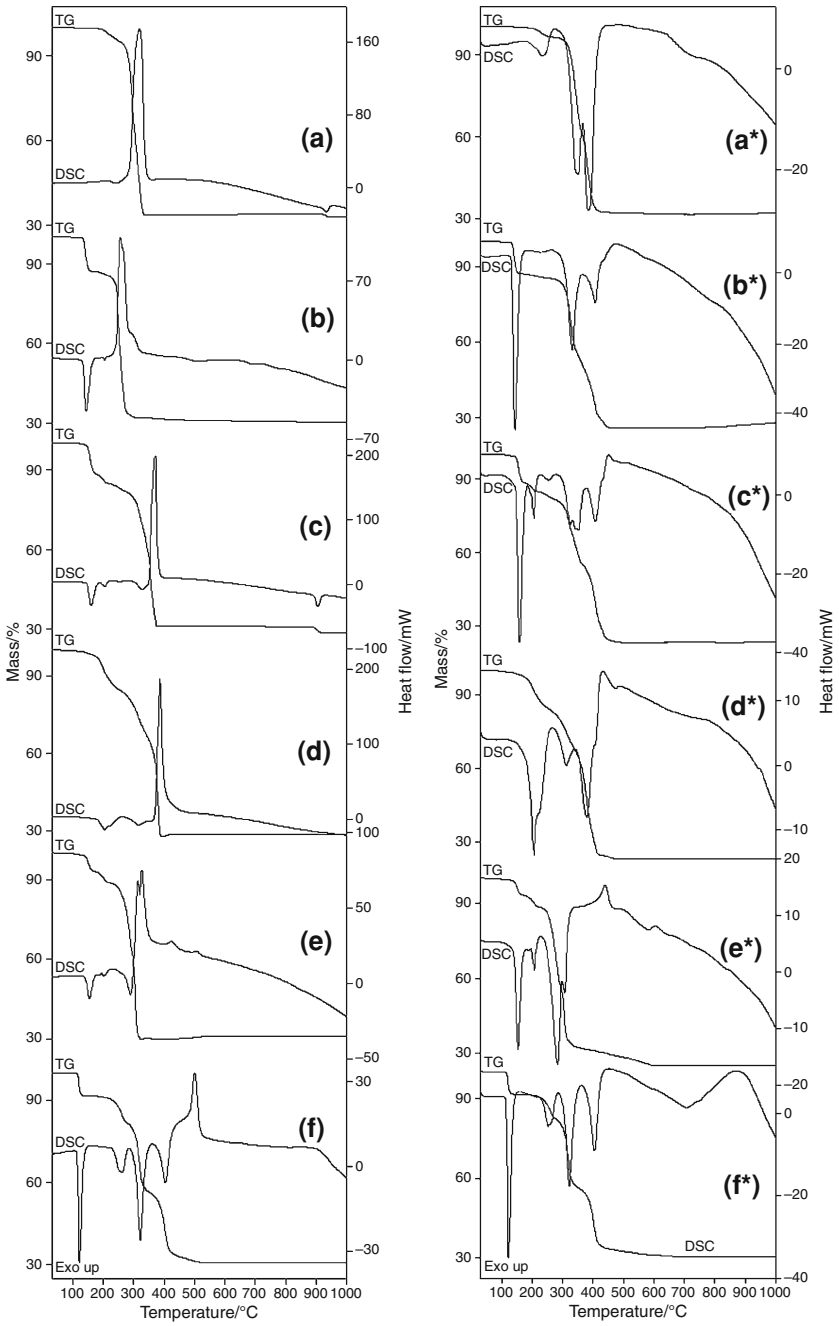

Fig. 7 TG-DSC curves of the compounds in dynamic air and N_2* atmospheres. **a**, **a*** MnL (m = 7.044 mg, 7.042 mg*). **b**, **b*** FeL·1H_2O (m = 7.142 mg, 7.116 mg*). **c**, **c*** CoL·1.5H_2O (m = 7.076 mg, 7.083 mg*). **d**, **d*** NiL·1.5H_2O (m = 7.129 mg, 7.068 mg*). **e**, **e*** CuL·1H_2O (m = 7.069 mg, 7.183 mg*). **f**, **f*** ZnL·1H_2O (m = 7.108 mg, 7.142 mg*)

sufficient to produce the thermal event. The total mass loss up to 600 °C is in agreement with the formation of Fe_2O_3, as final residue (Cald. = 70.20%, TG = 69.80%).

For the N_2 atmosphere, the thermal decomposition of the anhydrous compound also occurs in two steps between 180–330 and 330–450 °C with losses of 29.24 and 32.06%, corresponding to the endothermic peaks at 325 and 400 °C, respectively. The total mass loss (74.43%) up to 450 °C suggests the formation of a mixture of Fe and FeO in no simple stoichiometric relation. The mass gain (2.25%) observed between 750 and 1,000 °C without any thermal event in the DSC curve is attributed to the oxidation of the mixture Fe-FeO to FeO-Fe_3O_4. The oxidation in N_2 atmosphere occurs, probably, because the equipment is not hermetically sealed and/or trace of oxygen in N_2 which was used as purge gas.

Cobalt compound

The simultaneous TG-DSC curves in dynamic air and N_2 atmospheres are shown in Fig. 7c, c*, respectively. The first mass loss between 130 and 175 °C, corresponding to an

endothermic peak at 155 °C in both atmospheres is because of the dehydration with loss of $1.5H_2O$ (Calcd. = 10.31%, TG = 10.40% (air), 10.25% (N_2)).

For the air atmosphere, the thermal decomposition of the anhydrous compound occurs in three steps, with the last two overlapping ones, between 175–210, 210–340, and 340–365 °C, with losses of 3.97, 27.01, and 25.91%, corresponding to endothermic peaks at 205 and 320 °C and a large exothermic peak attributed to thermal decomposition and oxidation of the organic matter, respectively. The total mass loss up to 365 °C is in agreement with the formation of Co_3O_4 (Calcd. = 69.37%, TG = 69.19%). The last mass loss observed between 890 and 915 °C, corresponding to the endothermic peak at 900 °C is attributed to reduction reaction of Co_3O_4 to CoO (Calcd. = 1.97%, TG = 1.90%) and in agreement with the results of the Ref. [13].

For the N_2 atmosphere, the thermal decomposition of the anhydrous compound also occurs in three steps between 175–210, 210–350, and 350–450 °C, with losses of 4.11, 28.77, and 33.47%, corresponding to endothermic peaks at 205, 244, 313, 340, and 395 °C and exothermic one at 430 °C, showing that the thermal decomposition occurs with a large number of consecutive or simultaneous steps and through a more complex pathway than that observed from the TG curve. The total mass loss up to 450 °C (76.60%) suggests the formation of a mixture of Co and CoO in no simple stoichiometric relation.

Nickel compound

The simultaneous TG-DSC curves in dynamic air and N_2 atmospheres are shown in Fig. 7d, d*. In both atmospheres, the dehydration was firstly pointed out by their DSC curves and then determined from the corresponding mass losses observed in the TG curves. The mass loss between 100 and 215 °C, corresponding to an endothermic peak at 205 °C is due to dehydration with loss of $1.5H_2O$ (Calcd. = 10.32%, TG = 10.20% (air), 10.03% (N_2)).

For the air atmosphere, the thermal decomposition of the anhydrous compound occurs in the steps between 215–250, 250–350, and 350–380 °C, with losses of 4.70, 20.19, and 36.51%, corresponding to endothermic peaks at 225 (shoulder) and 310 °C attributed to the thermal decomposition and a large and sharp exothermic peak at 375 °C, attributed to the oxidation of the organic matter, with the formation of a mixture of Ni and NiO. The small mass gain between 380 and 420 °C is attributed to the oxidation reaction of Ni to NiO. The total mass loss up to 430 °C is in agreement with the formation of NiO, as final residue (Calcd. = 71.47%, TG = 71.60%).

For the N_2 atmosphere, the thermal decomposition of the anhydrous compound occurs in four steps between 215–250, 250–330, 330–410, and 410–465 °C, with losses of 5.59, 17.10, 42.72, and 1.77%, corresponding to the endothermic peaks at 225 (shoulder), 305, 370, and 460 °C, attributed to the thermal decomposition with the formation of Ni, as final residue (Calcd. = 77.58%, TG = 77.21%). The exothermic peak observed at 440 °C, after the third endothermic peak is attributed to the formation of formamide, which was identified in the gaseous products evolved and monitored by FTIR.

Copper compound

The simultaneous TG-DSC curves in dynamic air and N_2 atmospheres are shown in Fig. 7e, e*. The first mass loss between 100 and 165 °C, corresponding to an endothermic peak at 155 °C in both atmospheres is due to dehydration with loss of $1H_2O$ (Calcd. = 6.99%, TG = 6.84% (air), 6.70% (N_2)).

For the air atmosphere, the thermal decomposition of the anhydrous compound occurs in three steps, with the last two overlapping ones, between 165–210, 210–290, and 290–340 °C, with losses of 4.66, 26.94, and 30.56%, corresponding to the endothermic peaks at 200 and 285 °C, attributed to the thermal decomposition and exothermic ones at 305 and 325 °C, attributed to the oxidation of the organic matter, with the formation of a mixture of Cu_2O and CuO. The mass gain (1.05%) observed between 415 and 520 °C, corresponding to the exothermic peaks at 415 and 500 °C is attributed to the oxidation reaction of Cu_2O to CuO. The total mass loss up to 550 °C is in agreement with the formation of CuO, as final residue (Calcd. = 69.13%, TG = 69.00%).

For the N_2 atmosphere, the thermal decomposition of the anhydrous compound occurs in four steps, with the second and third overlapping ones, between 165–220, 220–290, 290–330, and 330–580 °C, with losses of 5.09, 31.10, 24.88, and 6.78%, corresponding to endothermic peaks at 200, 275, 300, and 570 °C and exothermic one at 430 °C attributed to the thermal decomposition with the formation of Cu as final residue (Calcd. = 75.34%, TG = 74.55%). The exothermic peak at 430 °C is due to the formation of isocyanic acid, cyanhydric acid, and formamide which were identified in the gaseous products evolved during the thermal decomposition and monitored by FTIR.

Zinc compound

The simultaneous TG-DSC curves in dynamic air and N_2 atmospheres are shown in Fig. 7f, f*. The first mass loss between 115 and 140 °C, corresponding to an endothermic peak at 130 °C in both atmospheres is due to dehydration with loss of $1H_2O$ (Calcd. = 6.94%, TG = 6.82%).

Table 3 Temperature ranges (θ) and the evolved products for each step of the TG-DSC curves in an air and N_2 atmospheres of the anhydrous compounds ML_2

	Compounds	Steps			
		First	Second	Third	Fourth
MnL2	θ/°C (air)	180–250	250–330		
	Evolved products	HNCO, CO_2	N_2O, NH_3, CO_2		
	θ/°C (N_2)	180–250	250–335	355–440	
	Evolved products	HNCO, CO, NH_3, CO_2, $HCONH_2$	NH_3, CO, CO_2, HCN, $HCONH_2$	CO_2, CO, NH_3, HCN	
FeL_2	θ/°C (air)	180–300	300–600		
	Evolved products				
	θ/°C (N_2)	180–330	330–450		
	Evolved products	NH_3, CO, CO_2, $HCONH_2$	NH_3, CO, CO_2, HCN, $HCONH_2$		
CoL_2	θ/°C (air)	175–210	210–340		
	Evolved products	NH_3, CO	CO, NH_3, CO_2, N_2O		
	θ/°C (N_2)	175–210	210–350		
	Evolved products	NH_3, CO	$HCONH_2$, HCN, NH_3, CO_2, CO		
NiL_2	θ/°C (air)	215–250	250–350	350–380	
	Evolved products	CO_2	NH_3, N_2O, CO, CO_2	N_2O, NH_3, CO, CO_2	
	θ/°C (N_2)	215–250	250–330	330–410	410–465
	Evolved products	NH_3	CO, CO_2, NH_3	CO, CO_2, NH_3	$HCONH_2$
CuL_2	θ/°C (air)	165–210	210–290	290–340	
	Evolved products	CO_2	CO2, CO, N_2O, HCN	HNCO, CO_2	
	θ/°C (N_2)	165–220	220–290	290–330	330–580
	Evolved products	CO, CO_2, NH_3, $HCONH_2$	CO, CO_2, NH_3, $HCONH_2$	CO_2, NH_3	NH_3, HCNO, HCN, $HCONH_2$
ZnL_2	θ/°C (air)	200–270	270–330	330–420	420–510
	Evolved products	CO, CO_2	CO, CO_2	CO_2, CO, HCN	CO_2, CO, N_2O, NH_3, HCN
	θ/°C (N_2)	200–270	270–330	330–420	420–700
	Evolved products	CO_2, NH_3, CO	CO_2, CO, NH_3, $HCONH_2$	CO_2, CO, NH_3, HCN	HCN, NH_3, $HCONH_2$

M transition metal, *L* oxamate

The thermal decomposition of the anhydrous compound in air atmosphere occurs in four steps between 200–270, 270–330, 330–420, and 420–510 °C, with losses of 9.71, 24.00, 25.07, and 3.23%, corresponding to the endothermic peaks at 255, 260, 320, and 400 °C attributed to the thermal decomposition and exothermic peak at 490 °C attributed to the oxidation of the organic matter. The total mass loss up to 510 °C is in agreement with the formation of ZnO, as final residue (Calcd. = 68.64%, TG = 68.83%).

For N_2 atmosphere, the thermal decomposition also occurs in four steps and in the same temperature range, except the last step that occurs between 420–700 °C, with losses of 8.90, 25.08, 24.54, and 3.51%, corresponding to the endothermic peaks at 250, 315, and 395 °C, attributed to the thermal decomposition with formation of ZnO, as final residue (Calcd. = 68.64%, TG = 68.59%).

The gaseous products released during the thermal decomposition in dynamic dry air and nitrogen atmospheres of the compounds examined in this study were monitored by FTIR, and they are shown in Table 3.

Conclusions

From TG, complexometry and elemental analysis data, a general formula could be established for the binary compounds involving some bivalent transition metal ions and with oxamate.

The experimental and theoretical infrared spectroscopic data suggest that the oxamate acts as a bidentate bond and the metal ions are coordinated by oxygen of the amide group and oxygen of the carboxylate one.

The TG-DSC coupled to infrared spectroscopy provided unreported informations concerning the thermal stability, as well as the gaseous products evolved during the thermal decomposition in dynamic dry air and nitrogen atmospheres.

The gaseous products released during the thermal decomposition of these compounds depend on the nature of the metal ion, as well as the atmosphere used, as shown in Table 3.

Acknowledgements The authors acknowledge to the Conselho Nacional de Desenvolvimento Científico e Tecnológico (CNPq), the Coordenação de Aperfeiçoamento de Pessoal de Nível Superior (CAPES) and the Fundação de Amparo à Pesquisa do Estado de São Paulo (FAPESP) for financial support. This research was supported by resources supplied by the Center for Scientific Computing (NCC/GridUNESP) of the Sao Paulo State University (UNESP), Instituto de Química de Araraquara, UNESP–Campus de Araraquara and CENAPAD-UNICAMP.

References

1. Wallace F, Wagner E. Infrared and far-infrared spectra of solid oxamic acid, deutero-oxamic acid and their salts. Spectrochim Acta A. 1978;34:589–606.
2. Perlepes SP, Zafiropoulos TF, Kouinis JK, Galinos AG. Complexes of zinc-group metals with oxamic acid. Inorg Nucl Chem Lett. 1980;16:475–80.
3. Shoeters G, Deleersnuder D, Desseyn HO. The complexes of oxamic acid with Ni(II). Spectrochim Acta A. 1983;39:71–6.
4. Allan JR, Dalrymple J. The thermal, spectral and magnetic studies of oxamic acid compounds of cobalt(II), nickel(II) and copper(II) ions. Thermochim Acta. 1993;221:199–204.
5. Vansant C, Desseyn HO, Perlepes SP. The synthesis, spectroscopic and thermal study of oxamic acid compounds of some metal(II) ions. Transition Met Chem. 1995;20:454–9.
6. Keuleers R, Janssens J, Desseyn HO. Thermal analysis of oxamates, thiooxamates and their complexes Part 1. The ligands. Thermochim Acta. 1998;311:149–54.
7. Keuleers R, Janssens J, Desseyn HO. Thermal analysis of oxamates, thiooxamates and their complexes Part 2. The Cu(II) complexes. Thermochim Acta. 1998;311:155–62.
8. Rodrigues-Martin Y, Ruiz-Pérez C, Gonzáles-Platas J, Sanchiz J, Lloret F, Julve M. A new eight-coordinate complex of manganese(II): synthesis, crystal structure, spectroscopy and magnetic properties of $[Mn(Hoxam)_2(H_2O)_4]$ (H_2 oxam_oxamic acid). Inorg Chim Acta. 2001;315:120–5.
9. Lemos SC, Franchi SJS, Netto AVG, Mauro AE, Treu-Filho O, Frem RCG, Almeida ET, Torres C. Synthesis, characterization, thermal studies, and DFT calculations on Pd(II) complexes containing *N*-methylbenzylamine. J Therm Anal Calorim. 2011. doi: 10.1007/s10973-011-1494-9.
10. Carvalho CT, Caires FJ, Lima LS, Ionashiro M. Thermal investigation of solid 2-methoxycinnamylidenepyruvate of some bivalent transition metal ions. J Therm Anal Calorim. 2011. doi: 10.1007/s10973-011-1679-2.
11. Kalinowska M, Swislocka R, Lewandowski W. The spectroscopic (FT-IR, FT-Raman, UV and 1H, 13C NMR) and theoretical studies of alkali metal *o*-methoxybenzoates. J Mol Struct. 2006;792–793:130–8.
12. Karabacak M, Cinar M, Kurt M. An experimental and theoretical study of molecular structure and vibrational spectra of 2-chloronicotinic acid by density functional theory and ab initio Hartree–Fock calculations. J Mol Struct. 2008;885:28–35.
13. Caires FJ, Lima LS, Carvalho CT, Giagio RJ, Ionashiro M. Thermal behaviour of malonic acid, sodium malonate and its compounds with some bivalent transition metal ions. Thermochim Acta. 2010;497:35–40.
14. Flaschka HA. EDTA titrations. 2nd ed. Oxford: Pergamon Press; 1964.
15. Oliveira CN, Ionashiro M, Graner CAF. Titulação complexométrica de zinco, cobre e cobalto. Ecl Quim. 1985;10:7–10.
16. Becke AD. Density-functional thermochemistry III. The role of exact exchange. J Chem Phys. 1993;98:5648–52.
17. Lee C, Yang W, Parr RG. Development of the Colle-Salvetti correlation-energy formula into a functional of the electron density. Phys Rev B Condens Matter Mater Phys. 1988;37:785–9.
18. Mclean AD, Chandler GS. Contracted Gaussian basis sets for molecular calculations. I. Second row atoms, Z = 11–18. J Chem Phys. 1980;72:5639–48.
19. Krishnan R, Binkley JS, Seeger R, Pople JA. Self-consistent molecular orbital methods. XX. A basis set for correlated wave functions. J Chem Phys. 1980;72:650–4.
20. Frisch MJ, Trucks GW, Schlegel HB, Scuseria GE, Robb MA, Cheeseman JR, Scalmani G, Barone V, Mennucci B, Petersson GA, Nakatsuji H, Caricato M, Li X, Hratchian HP, Izmaylov AF, Bloino J, Zheng G, Sonnenberg JL, Hada M, Ehara M, Toyota K, Fukuda R, Hasegawa J, Ishida M, Nakajima T, Honda Y, Kitao O, Nakai H, Vreven T, Montgomery JrJA, Peralta J E, Ogliaro F, Bearpark M, Heyd JJ, Brothers E, Kudin KN, Staroverov VN, Kobayashi R, Normand J, Raghavachari K, Rendell A, Burant JC, Iyengar SS, Tomasi J, Cossi M, Rega N, Millam NJ, Klene M, Knox JE, Cross JB, Bakken V, Adamo C, Jaramillo J, Gomperts R, Stratmann RE, Yazyev O, Austin AJ, Cammi R, Pomelli C, Ochterski JW, Martin RL, Morokuma K, Zakrzewski VG, Voth GA, Salvador P, Dannenberg JJ, Dapprich S, Daniels AD, Farkas Ö, Foresman JB, Ortiz JV, Cioslowski J, Fox DJ. Gaussian 09, Revision A.02 Gaussian Inc. Wallingford CT. 2009.
21. Goodson DZ, Sarpal SK, Wolfsberg M. Influence on isotope effect calculations of the method of obtaining force constants from vibrational data. J Chem Phys. 1982;86:659–63.
22. GaussView, Version 5.0.8, Dennington R, Keith T, Millam J. *Semichem Inc.*, Shawnee Mission KS, 2000–2008.
23. Sundaraganesan N, Ilakiamani S, Joshua BD. FT-Raman and FT-IR spectra, ab initio and density functional studies of 2-amino-4,5-difluorobenzoic acid. Spectrochim Acta A. 2007;67:287–97.